Synthesis and Crystal Structure of Zr_2Te. Distinctions in Bonding to Isotypic Sc_2Te and the Relationship to the Structures of Congeneric Hf_2Te and Zr_2Se

Gissur Örlygsson and Bernd Harbrecht*

Department of Chemistry and Materials Science Centre, Philipps University, D-35032 Marburg, Germany

Received January 6, 1999

Zr_2Te is accessible by high-temperature synthesis. The structure of the zirconium-rich telluride was determined by means of powder X-ray diffraction to be orthorhombic, *Pnma* (No. 62), $Z = 12$, Pearson symbol *oP*36, $a =$ 1995.0(2) pm, $b = 382.36(2)$ pm, $c = 1065.63(9)$ pm. Pairwise interpenetrating columns of *trans*-face-shared, centered Zr_9 cuboids, reminiscent of the bcc high-temperature form of zirconium can be recognized as the topologically characteristic structural feature. Tellurium atoms capping the remaining square faces complete the motif of a $^1_\infty[Zr_8Te_4]$ double string running parallel [010]. The tellurium atoms are 7-, 8- and 9-fold coordinated by zirconium. The coordination figures represent mono-, bi- and tricapped distorted trigonal prisms, with zirconium atoms capping the square faces of the prisms. Extended Hückel calculations revealed distinctions in bonding in Zr_2Te and the isotypic Sc_2Te. According to Mulliken overlap populations, the heteronuclear interactions are similar in both tellurides. However, the lower valence electron concentration available for M−M bonding in Sc_2Te is reflected in a considerable restriction of the attractive homonuclear interactions to one-dimensional metal cores, whereas in Zr_2Te M−M bonding regions extend in space. The structure of Zr_2Te is contrasted with two other types of bcc fragment structures adopted by the congeneric Hf_2Te and Zr_2Se. We show that the structural diversity observed for various dimetal chalcogenides is controlled by an intimate interplay of electronic and geometric factors.

Introduction

In the past, a substantial number of binary metal-rich chalcogenides of the valence-electron-poor transition metals have been synthesized and characterized, e.g., Ti_8S_3,[1] Zr_2S,[2,3] Hf_2Se,[2] α- and β-V_3S,[4] Nb_2Se,[5] and Ta_2S.[6] The number of identified compounds in this category continues to grow. More recently discovered phases are, e.g., Sc_8Te_3,[7] Sc_2Te,[8] Y_8Te_3,[7] Ti_9Se_2,[9] $Ti_{11}Se_4$,[10] Ti_8Se_3,[11] β-Ti_2Se,[12] Zr_3Te,[13] Hf_2Te,[14] Hf_3Te_2,[15] Ta_2Se,[16] $Ta_{97}Te_{60}$,[17,18] $Ta_{181}Te_{112}$,[17,18] and dodecagonal (dd) $Ta_{1.6}Te$.[19,20] Of these, the phases Sc_2Te, Ti_9Se_2, $Ti_{11}Se_4$, Hf_3Te_2, Ta_2Se, and the tantalum tellurides account for new, previously unknown structure types. Sc_2Te, Ti_9Se_2, and $Ti_{11}Se_4$ have as a common structural feature strings of M_6 octahedra connected in various ways according to the concept of condensed clusters.[21] Hf_3Te_2 and Ta_2Se represent layered materials with bcc-like metal stacks coated on both sides with chalcogen atoms. The Te-3Hf-Te and Se-4Ta-Se layers, respectively, are held together by weak interactions. dd-$Ta_{1.6}Te$ is the first identified quasicrystalline chalcogenide; $Ta_{97}Te_{60}$ and $Ta_{181}Te_{112}$ are its crystalline approximants. The M_8Te_3 compounds of the third group elements Sc and Y[7] possess a particularly low number of valence electrons available for metal−metal bonding and are among the most metal-rich chalcogenides reported for the valence-electron-poor transition metals. Compared to the isostructural but valence-electron-richer Ti_8Q_3 (Q = S, Se) phases,[1,11] distinctive differences in structure as well as chemical bonding were observed. The underlying reasons were discussed, emphasizing cooperative matrix and bonding effects based on differences in atomic sizes and valence electron concentration.[7] In the present paper we report the crystal and electronic structures of the new subtelluride Zr_2Te,[22] which crystallizes isostructurally with Sc_2Te. Since both compounds are tellurides and the atomic radii of zirconium and scandium are very close to one another so as to minimize matrix effects, the comparison of the bonding situation in Zr_2Te and Sc_2Te becomes especially instructive.

(1) Owens, J. P.; Franzen, H. F. *Acta Crystallogr.* **1974**, *B30*, 427.
(2) Franzen, H. F.; Smeggil, J.; Conard, B. R. *Mater. Res. Bull.* **1967**, *2*, 1087.
(3) Yao, X.; Franzen, H. F. *J. Less-Common Met.* **1988**, *142*, L27.
(4) Pedersen, B.; Grønvold, F. *Acta Crystallogr.* **1959**, *12*, 1022.
(5) Conard, B. R.; Norrby, L. J.; Franzen, H. F. *Acta Crystallogr.* **1969**, *B25*, 1729.
(6) Franzen, H. F.; Smeggil, J. *Acta Crystallogr.* **1969**, *B25*, 1736.
(7) Maggard, P. A.; Corbett, J. D. *Inorg. Chem.* **1998**, *37*, 814.
(8) Maggard, P. A.; Corbett, J. D. *Angew. Chem.* **1997**, *109*, 2062; *Angew. Chem., Int. Ed. Engl.* **1997**, *36*, 1974.
(9) Weirich, T. E.; Simon, A.; Pöttgen, R. *Z. Anorg. Allg. Chem.* **1996**, *622*, 630.
(10) Weirich, T. E.; Ramlau, R.; Simon, A.; Hovmöller, S.; Zou, X. *Nature* **1996**, *382*, 144.
(11) Weirich, T. E.; Pöttgen, R.; Simon, A. *Z. Kristallogr.* **1996**, *211*, 929.
(12) Weirich, T. E.; Hovmöller, S.; Simon, A. *Nordic Structural Chemistry Meeting*, 16th, Sigtuna, Sweden, 1998; P44.
(13) Harbrecht, B.; Leersch, R. *J. Alloys Compd.* **1996**, *238*, 13.
(14) Harbrecht, B.; Conrad, M.; Degen, T.; Herbertz, R. *J. Alloys Compd.* **1997**, *255*, 178.
(15) Abdon, R. L.; Hughbanks, T. *Angew. Chem.* **1994**, *106*, 2414; *Angew. Chem., Int. Ed. Engl.* **1994**, *33*, 2328.
(16) Harbrecht, B. *Angew. Chem.* **1989**, *101*, 1696; *Angew. Chem., Int. Ed. Engl.* **1989**, *28*, 1660.
(17) Conrad, M. *Tantalreiche Telluride*. Thesis, University of Dortmund (Shaker Verlag: Aachen, Germany), 1997.
(18) Conrad, M.; Harbrecht, B. *Aperiodic '97*; de Boissieu, M., Currat, R., Verger-Gaugry, J.-L., World Scientific: Singapore, 1998.
(19) Conrad, M.; Krumeich, F.; Harbrecht, B. *Angew. Chem.* **1998**, *110*, 1454; *Angew. Chem., Int. Ed. Engl.* **1998**, *37*, 1383.
(20) Krumeich, F.; Conrad, M.; Nissen, H.-U.; Harbrecht, B. *Philos. Mag. Lett.* **1998**, *78*, 357.
(21) Simon, A. *Angew. Chem.* **1981**, *93*, 23; *Angew. Chem., Int. Ed. Engl.* **1981**, *20*, 1.
(22) Örlygsson, G.; Harbrecht, B. *Z. Kristallogr.* **1998**, *Suppl. 15*, 50.

10.1021/ic990024a CCC: $18.00
Published on Web 06/18/1999

Apart from the metal-rich phases Zr_2Te and Zr_3Te,[13] the latest investigations in the Zr−Te system have brought to light $Zr_{1.30}Te_2$,[23] and the recently discovered Zr_5Te_6,[24] adopting a NiAs type-related structure.

Experimental Section

Preparation. Due to their air-sensitivity, the tellurides were handled and stored under argon. The first indications of a new phase intermediate between Zr_5Te_4[25−27] and Zr_3Te[13] were obtained in arc-melting experiments: in as-cast samples of composition $0.71 < x_{Zr} < 0.79$ an additional phase, now identified as Zr_2Te, was present along with Zr and Zr_3Te.[13] Zr_2Te could also be synthesized through the reduction of Zr_5Te_4 with elemental Zr in the solid state (1170−1600 K), although not in a pure form. A better enrichment of the phase (>90%) was achieved by inductive heating, starting with the elements (Te, 99.999%, Fluka; Zr, 99.9%, Ventron, $n_{Zr}:n_{Te} = 2:1$, in total ca. 300 mg, 5 min), in sealed, argon-filled Ta tubes at 1970 K in a vacuum ($P < 10^{-3}$ Pa), with subsequent quenching by radiative heat loss.

Energy dispersive analysis of emitted X-rays (CamScan CS 4DV, EDX system, Noran Instruments; 30 kV, Zr-L, Te-L, Ta-L) on two different samples (six measurements) gave the composition $Zr_{2.0(1)}Te$. In addition, small amounts of Ta were detected, with the mole fraction observed in separate measurements on different as well as identical probes strongly fluctuating ($<x_{Ta}> = 0.013(0.008)$). Furthermore, a reciprocal relationship was observed between the acceleration voltage and the detected Ta contents. Thus, we assume the detected Ta to be a surface phenomenon. Providing further support for this assumption are the lattice parameters of Zr_2Te from samples where Ta contamination can be ruled out, which do not systematically deviate from those of Zr_2Te prepared in Ta tubes.

Powder X-ray Diffraction. Guinier X-ray powder diffraction was used as a characterization method for phase identification. Guinier photographs were obtained with a Huber Guinier System 600 employing Cu $K\alpha_1$ radiation. Silicon[28] was added to the samples as an internal standard. Lattice parameters were determined from Guinier diffraction data by least-squares refinement. X-ray powder diffractograms were recorded at ambient temperature on a computer-automated diffractometer (Siemens, D500), equipped with a diffracted-beam focusing graphitic monochromator, using Cu $K\alpha_1$ and $K\alpha_2$ radiation (50 kV, 30 mA). Intensities were detected by means of a scintillation counter. The data were processed with the local program DIFFRAKT.[29] Indexing of the diffraction pattern of Zr_2Te was accomplished with use of the program TREOR.[30] The lattice parameters and diffraction intensities suggested a phase isotypic with Sc_2Te.[8] As no single crystals of Zr_2Te could be obtained, the structural parameters were refined from a fit of the diffraction profile of a sample containing less than 2.5% weight fraction each of $Zr_{1-x}Te_x$, Ta, and Te, determined according to Hill and Howard.[31] The air-sensitive, reflection-rich Zr_5Te_4, initially present in the sample as a minor component, was allowed to decompose under atmospheric conditions into crystalline Te and an X-ray amorphous phase. The refinements were carried out using the modified Rietveld version LHPM,[32−34] applying a pseudo-Voigt profile fit. Atomic positions of the minority components were obtained from the literature (Zr and Ta,[35] Te[36]). The lattice parameters for Zr_2Te, $Zr_{1-x}Te_x$, and Ta were obtained from Guinier data. The lattice parameters of Zr_2Te and those of the isostructural compounds Sc_2Te[8] and β-Ti_2Se[12] are given in Table 1. Atomic positions of Sc_2Te were used as a starting set for Zr_2Te in the Rietveld refinement. Relevant parameters are summarized in Table 2. An X-ray powder diffractogram and the profile fit are shown in Figure 1. Positional parameters are listed in Table 3. Displacement parameters were separately refined for the Zr and Te atoms.

Table 1. Comparison of Lattice Parameters (pm) and Cell Volumes (10^6 pm^3) for Known Phases Crystallizing in the Sc_2Te Structure Type

compd	*a*	*b*	*c*	*V*
β-Ti_2Se[a]	1793.4(20)	345.3(1)	952.6(10)	590(2)
Zr_2Te	1995.0(2)	382.36(2)	1065.63(9)	812.9(2)
Sc_2Te[b]	2017.8(5)	391.86(7)	1067.5(2)	844.1(5)

[a] Reference 12. [b] Reference 8.

Table 2. Relevant Parameters of the Rietveld Analysis of Zr_2Te[a]

empirical formula	Zr_2Te
fw (g mol^{-1})	310.048
space group (No.); Z	*Pnma* (62); 12
$\rho_{rö}$ (g cm^{-3})	7.600
angular range; step size (2θ, deg)	8.5−85.0; 0.02
no. of phases	4
no. of variables (structural, Zr_2Te)	54 (20)
no. of reflcns	698
preferred orientation: direction; parameter	[010]; 1.271(6)
asymmetry parameter	0.8(1)
R_B[b]; R_p[c]; R_{wp}[d]	0.056; 0.110; 0.143

[a] Lattice parameters in Table 1. [b] $R_B = \sum|I_{ko} - I_{kc}|/\sum|I_{ko}$. [c] $R_p = \sum|y_{io} - y_{ic}|/\sum|y_{io}$. [d] $R_{wp} = [(\sum w_i(y_{io} - y_{ic})^2/(\sum w_i y_{io}^2)]^{1/2}$.

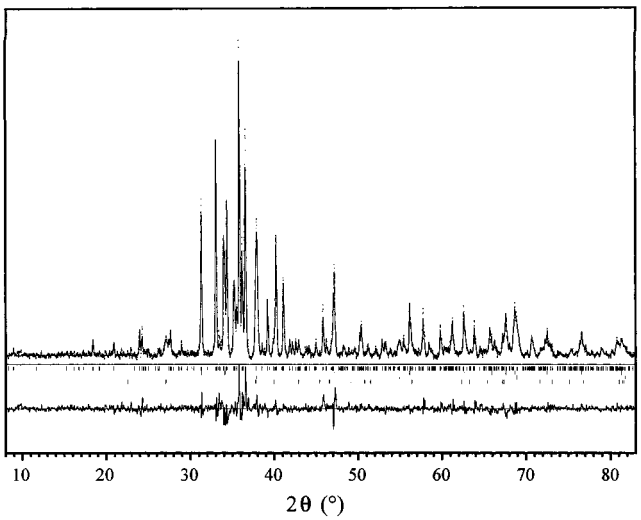

Figure 1. X-ray powder diffractogram (rel intensities vs 2θ) and a Rietveld profile fit of Zr_2Te and the minority components $Zr_{1-x}Te_x$, Ta, and Te. Measured (dots) and calculated (line) intensities with a difference plot (bottom). In the middle are shown the positions of the Bragg angles of Zr_2Te, $Zr_{1-x}Te_x$, Ta, and Te (top to bottom).

Electronic Structure Calculations. Band structure calculations on Zr_2Te and Sc_2Te were carried out within the tight-binding approximation, at 48 k points, using the extended Hückel method.[37−39] Valence-state ionization energies (H_{ii}'s) for Zr were obtained from a charge-iterative calculation on Zr_2Te. Other parameters have been cited elsewhere.[8,40] The parameters are listed in Table 4.

(23) Wang, C.; Eylem, C.; Hughbanks, T. *Inorg. Chem.* **1998**, *37*, 390.
(24) Örlygsson, G.; Harbrecht, B. *Z. Kristallogr.* **1999**, *Suppl. 16*, 52.
(25) Brattås, L.; Kjekshus, A. *Acta Chem. Scand.* **1971**, *25*, 2350.
(26) de Boer, R.; Cordfunke, E. H. P.; van Vlaanderen, P.; Ijdo, D. J. W.; Plaisier, J. R. *J. Solid State Chem.* **1998**, *139*, 213.
(27) Örlygsson, G.; Harbrecht, B. *Z. Kristallogr.—NCS* **1999**, *214*, 5.
(28) Deslattes, R. D.; Henins, A. *Phys. Rev. Lett.* **1976**, *36*, 898.
(29) Wagner, V.; Degen, T. *DIFFRAKT (V1.0): A program for processing X-ray powder data*; University of Bonn: Germany, 1995.
(30) Werner, P. E. *TREOR: Trial and error program for indexing of unknown powder patterns*; University of Stockholm: Sweden, 1988.
(31) Hill, R. J.; Howard, C. J. *J. Appl. Crystallogr.* **1987**, *20*, 467.
(32) Rietveld, H. M. *J. Appl. Crystallogr.* **1969**, *2*, 65.
(33) Wiles, D. B.; Young, R. A. *J. Appl. Crystallogr.* **1981**, *14*, 149.
(34) Howard, C. J.; Hill, R. J. *AAEC Rep. M112*, 1986.
(35) Villars, P. *Pearson's Handbook, Desk Edition*; American Society for Metals: Materials Park, OH, 1997; Vol. 2.
(36) Cherin, P.; Unger, P. *Acta Crystallogr.* **1967**, *23*, 670.
(37) Hoffmann, R. J. *J. Chem. Phys.* **1963**, *39*, 1397.
(38) Whangbo, M.-H.; Hoffmann, R. J. *J. Am. Chem. Soc.* **1978**, *100*, 6093.
(39) Köckerling, M. *Program EHMACC*, adapted for use on PC by M. Köckerling; Gesamthochschule Duisburg: Germany, 1997.
(40) Clementi, E.; Roetti, C. *At. Data Nucl. Data Tables* **1974**, *14*, 177.

Table 3. Atomic Coordinates and Isotropic Thermal Parameters (B_{iso} (10^4 pm^2)) of Zr_2Te[a]

atom	x	z	B_{iso}[b]
Te1	0.0731(3)	0.8392(6)	1.5(2)
Te2	0.3696(3)	0.7190(6)	1.5(2)
Te3	0.2605(3)	0.0398(6)	1.5(2)
Zr1	0.3951(4)	0.1499(8)	0.56(14)
Zr2	0.3421(4)	0.4580(8)	0.56(14)
Zr3	0.2270(4)	0.7487(8)	0.56(14)
Zr4	0.0348(4)	0.1088(8)	0.56(14)
Zr5	0.1456(4)	0.4218(8)	0.56(14)
Zr6	0.4845(4)	0.8890(8)	0.56(14)

[a] All atoms in position 4*c* with $y = {}^1/_4$. [b] $B_{iso} = 8\pi^2U^2$.

Table 4. Parameters Used for Extended Hückel Calculations

	orbital	H_{ii} (eV)	ζ_1[a]	c_1[b]	ζ_2[a]	c_2[b]
Zr	5s	−7.33	1.82			
	5p	−3.84	1.78			
	4d	−6.91	3.84	0.6213	1.505	0.5798
Sc	4s	−6.74	1.30			
	4p	−3.38	1.30			
	3d	−6.12	4.35	0.4228	1.700	0.7276
Te	5s	−21.20	2.51			
	5p	−12.00	2.16			

[a] Slater-type orbital exponents. [b] Coefficients used in double-ζ expansion.

Results and Discussion

Phase Relations. The lattice parameters found for Zr_2Te prepared with varying nominal composition of the reaction mixture gave no indication of a homogeneity range. According to DTA (Differential Thermal Analysis) measurements[41] there exists a eutectic at 1616 ± 3 K in mixtures of Zr and Zr_3Te at 21 at. % Te. De Boer and Cordfunke[41] found Zr_3Te to melt incongruently at 1627 ± 6 K to give Zr_5Te_4 and liquid. Zr_2Te was not observed, however, they reported difficulties in assigning the enthalpy effects near 35 at. % Te. One reason for this might be their method of synthesis used,[41] which most likely leads to minimal amounts of Zr_2Te being produced. Thus, during the heating part (10 K min^{-1}) of the first DTA cycle one could not expect the enthalpy effect of Zr_2Te to be observed. On cooling from 1925 K at a rate of 10 K min^{-1} we would however expect the peritectic formation of solid Zr_2Te to be observed in a small temperature interval some degrees above the incongruent melting point of Zr_3Te. This circumstance has to be elucidated in further experiments.

Structural Features. Zr_2Te crystallizes in the Sc_2Te type structure[8] in the orthorhombic space group *Pnma*. The structure is composed of nine crystallographically inequivalent atoms, Zr1−Zr6 and Te1−Te3, all of which lie in mirror planes located at heights $y = {}^1/_4, {}^3/_4$ modulo 1. Interatomic distances are listed in Table 5. As emphasized in the projection of the Zr_2Te structure along [010] in Figure 2a, four of the six crystallographically distinct Zr atoms (Zr1, Zr4, Zr5, Zr6) topologically represent a metal partial structure (Figure 3a), which is reminiscent of the bcc-Zr structure stable above 1139 K.[42] Pairwise interpenetrating columns of *trans*-face-shared, centered Zr_9 cuboids with additional Te atoms above the square faces extend along [010] presenting the motif of a ${}^1_\infty[Zr_8Te_4]$ double string. Accordingly, the *b* parameter (382.4 pm) is related to the cell parameter of bcc-Zr (360.9 pm at 1252 K).[43] In the metal core of the structure (Zr1, Zr5, Zr6), the Zr1−Zr6 and Zr6−Zr6 contacts (310 pm) are shorter than the closest contact in the metal itself (d_{bcc} = 313 pm; d_{hcp} = 318 pm).[42] Other contacts in the core unit range from 320 to 379 pm. Alternatively, in compliance with Simon's concept of condensed clusters,[21] the columnar fragments also represent chains of distorted octahedral Zr_6Te_8 clusters with Zr atoms replacing four of the eight Te atoms. Each octahedron is condensed via *cis*-standing edges to two others, resulting in double chains of the columnar fragments. The double chains are further linked along [001] via homonuclear Zr4−Zr4 contacts (331 pm), as shown in Figure 6b. The metal atoms on the remaining two sites, Zr2 and Zr3, can be viewed as forming a zigzag chain along [010] with $d_{Zr2-Zr3}$ = 325 pm. Note, that this chain can also be seen as a part of another type of a columnar bcc fragment built up by Zr2 and Zr3 together with Zr1 and Zr5 of two separate double chains. Two further bcc fragments can be detected in the structure: Zr3 connecting to Zr1 and Zr5, and thereby forming a part of the bcc structure in the double chains, and, a fragment built up by Zr2 and two Zr4. These fragments, along with the double chain, can in part be recognized in Figure 2b, where Zr atom pairs with Mulliken overlap population (MOP) values >0.090 (vide infra) are connected.

The Te atoms are 7-, 8-, and 9-fold (Te2, Te3, and Te1, respectively) coordinated by Zr, the coordination figures representing mono-, bi-, and tricapped distorted trigonal prisms, with Zr atoms capping the square faces of the prisms (Figure 3b). The bi- and tricapped trigonal prisms are fused along [010] by sharing of triangular Zr_3 faces. These fragments are condensed via common edges, building twin columns of capped trigonal prisms running along [010] (see Figure 6b). The monocapped prisms lie perpendicular to the others, sharing edges, and thereby building columns along [010] of opposedly oriented prisms with every other prism centered with a Te atom. An examination of the average Zr−Te distances in the capped, Te centered trigonal prisms, amounting to 293.2 pm (Te1), 290.2 pm (Te2), 297.2 pm (Te3), and 293.5 pm in the average, reveals a close resemblance to the Te coordination figures in the contiguous phases Zr_3Te and Zr_5Te_4. In Zr_3Te,[13] where solely tricapped trigonal prisms are observed, the corresponding average distance is 294.5 pm, and, in Zr_5Te_4,[27] where the Te coordination figure constitutes a *hypho*-Zr_6Te fragment of a tricapped trigonal prism, this distance is 295.1 pm. The shortest Te−Te contact in Zr_2Te is 375 pm (Te2−Te3), well above the second nearest neighbor distance in elemental Te (349.5 pm).[36]

Electronic Structure: Comparison with Sc_2Te. According to the total DOS diagrams for Zr_2Te and the isotypic Sc_2Te shown in Figure 4, the Fermi level lies in both cases in regions that are dominated by Sc and Zr d orbital contributions. Hence, both materials should have metallic properties. The Fermi level in Sc_2Te lies near the top of a peak in the DOS whereas in Zr_2Te it lies near a local minimum. The greater dispersion of the projected Zr 4d states around the Fermi level compared to the Sc 3d states can be related to a greater interaction integral[44] of the Zr atoms in Zr_2Te. Using the cohesive energy of the metal as an indicator for the interaction integral, the dispersions of the projected 3d and 4d states of Sc and Zr, respectively, reflect the difference in the enthalpies of atomization: $\Delta_a H^\circ_{298}(Zr)$ = 608.8 kJ/mol; $\Delta_a H^\circ_{298}(Sc)$ = 377.8 kJ/mol.[45] This difference leads to slightly shorter homonuclear metal−metal mean distances in Zr_2Te, expressing itself mainly in the shorter *b* axis.

(41) de Boer, R.; Cordfunke, E. H. P. *J. Alloys Compd*. **1997**, *259*, 115.
(42) Guillermet, A. F. *High Temp.-High Press*. **1987**, *19*, 119.
(43) Skinner, G. B.; Johnston, H. L. *J. Chem. Phys.* 1**953**, *21*, 1383.
(44) Burdett, J. K. *Chemical Bonding in Solids*; Oxford University Press: New York, 1995.
(45) Weast, R. C., Ed. *Handbook of Chemistry and Physics*, 1st student edition; CRC Press: Boca Raton, FL, 1988.

Table 5. Relevant Interatomic Distances and Mulliken Overlap Populations (MOP) for Zr_2Te (MOP Values in Square Brackets Refer to Sc_2Te)

atom no.			d (pm)	MOP	atom no.			d (pm)	MOP
M6	M6	2×	310.3(9)	0.406 [0.362]	M2	M5	1×	394(1)	0.040 [−]
M1	M6	2×	309.9(9)	0.354 [0.228]	M2	M3	1×	386(1)	0.039 [0.013]
M1	M6	1×	330(1)	0.291 [0.167]	M5	M5	2×	382.36(2)	0.032 [−]
M1	M5	2×	319.7(9)	0.290 [0.174]	M4	M5	1×	400(1)	0.029 [0.008]
M5	M6	2×	324.2(9)	0.276 [0.146]					
M2	M3	2×	324.5(1)	0.274 [0.086]	M3	Te2	1×	286(1)	0.357 [0.296]
M4	M4	2×	331.1(1)	0.223 [0.028]	M2	Te2	1×	284(1)	0.356 [0.320]
M1	M3	2×	327.1(9)	0.212 [0.121]	M2	Te1	2×	285.0(8)	0.323 [0.274]
M2	M4	2×	350.2(1)	0.134 [0.015]	M5	Te2	2×	290.1(8)	0.315 [0.254]
M1	M2	1×	345(1)	0.131 [0.072]	M2	Te3	2×	293.4(8)	0.307 [0.283]
M5	M6	1×	379(1)	0.117 [0.174]	M4	Te2	2×	294.5(8)	0.301 [0.280]
M4	M6	2×	356.7(1)	0.108 [0.036]	M1	Te1	2×	285.1(8)	0.297 [0.234]
M6	M6	2×	382.36(2)	0.101 [0.045]	M3	Te3	2×	294.5(8)	0.290 [0.225]
M3	M3	2×	382.36(2)	0.100 [0.036]	M5	Te3	2×	295.7(8)	0.280 [0.236]
M3	M5	2×	367.6(1)	0.095 [0.009]	M4	Te1	2×	293.2(8)	0.279 [0.273]
M1	M1	2×	382.36(2)	0.064 [0.018]	M6	Te2	1×	292(1)	0.266 [0.239]
M1	M4	1×	379(1)	0.060 [0.026]	M1	Te3	1×	293(1)	0.249 [0.246]
M4	M4	2×	382.36(2)	0.056 [−]	M4	Te1	1×	297(1)	0.249 [0.267]
M2	M2	2×	382.36(2)	0.052 [−]	M6	Te1	1×	301(1)	0.194 [0.127]
M3	M5	1×	384(1)	0.045 [0.010]	M3	Te3	1×	317(1)	0.161 [0.173]
M2	M4	1×	391(1)	0.042 [−]	M3	Te1	1×	322(1)	0.112 [0.073]

The Te p orbital contributions lie in both cases almost exclusively in the region between −14.5 and −11 eV. There are also small Te p orbital contributions well above the Fermi level.

The crystal orbital overlap population (COOP) curves (Figure 4) for heteronuclear metal−tellurium interactions show comparable bonding behavior for both compounds. On the other hand, it can be seen that homonuclear metal−metal d orbital interactions are much more pronounced, and that fewer metal−metal bonding states remain unoccupied in Zr_2Te than in Sc_2Te. As the 4d orbitals of Zr are, compared to the 3d orbitals of Sc, more diffuse and more exposed, and considering the difference in valence electron concentration *vec* available for metal−metal bonding in the two materials (Zr_2Te, *vec* = 3; Sc_2Te, *vec* = 2), this can be anticipated. In the region between −14.5 and −11 eV there are minor Zr−Zr bonding interactions, whereas in this region bonding and antibonding Sc−Sc interactions cancel out.

The Mulliken overlap population (MOP) for a given pair of atoms can be seen as an expression for the strength of bonding interactions. MOP values for pairs of atoms in both structures are listed in Table 5, for Zr_2Te according to decreasing MOP, with a parallel listing of the corresponding values for Sc_2Te. In plotting MOP vs d_{M-M} and MOP vs d_{M-Te} for metal−metal and metal-tellurium pairs respectively, the distinctions in homonuclear and heteronuclear bonding are demonstrated (Figure 5). The MOP values for metal−tellurium interactions scatter around a common straight line, with bond length being inversely proportional to bond strength. In contrast, the MOP values for homonuclear metal−metal interactions scatter around two separate curves. Considering the near coincidence of the MOP vs d_{M-Te} curves for both structures, we conclude that the distinct MOP vs d_{M-M} curves reflect differing MOP values at a given distance rather than differing interatomic distances at a given MOP value.

A qualitative comparison of the two diagrams in Figure 5 gives an idea of the greater importance of metal−tellurium interactions for Sc_2Te over Zr_2Te, or, conversely, the greater importance of metal−metal interactions in Zr_2Te over Sc_2Te. Exploring this point further, it can be seen from Table 5 that the Sc−Sc overlap populations around Sc2, Sc3, and Sc4, the Sc atoms with the most Te neighbors, namely five, are small, much smaller than the corresponding values in Zr_2Te. Compare for example the metal pairs (d_{Zr-Zr}, pm) 2−3 (324.5), 3−5 (367.6), 4−4 (331.1), 2−4 (350.2), and 4−6 (356.7). Sc2, Sc3, and Sc4 are strongly oxidized through Te and, as opposed to the equivalent Zr atoms, lack valence electron density in order to enter into extensive bonding interactions with the surrounding Sc atoms. They will therefore, compared to the equivalent Zr atoms, be to a much greater extent fixed in place by heteronuclear rather than homonuclear covalent interactions. The bonding electrons of Sc1, Sc5, and Sc6, on the other hand, seem to be more or less delocalized inside the core unit built up by these very atoms, leading to extended metal−metal bonding interactions inside this unit.

An anomaly regarding the Sc1−Sc6 (348.6 pm) and Sc5−Sc6 (351.9 pm) interactions becomes evident in the MOP vs d_{M-M} diagram of Figure 5. Compared to the Zr1−Zr6 coordinate, the Sc1−Sc6 coordinate is shifted toward a lower overlap population and a longer distance. Opposedly, the values for Sc5−Sc6 are shifted to a higher overlap population and a shorter interatomic distance. A tentative explanation would be the increased metal coordination of M1 through M2 and M3, as compared to the metal coordination of M5. In the case of electron-poor Sc this could lead to some weakening of the interaction of Sc1 with Sc6. As a consequence, the long Sc1−Sc6 distance then would allow Sc5 to interact more closely with Sc6.

In summary, on the basis of the extended Hückel calculations, it can be said that in Zr_2Te the metal−metal bonding interactions spread throughout the whole body of the structure, as shown in Figure 2b, building an extensive network, whereas in Sc_2Te the metal−metal interactions are concentrated on the core unit leaving other parts of the structure dominated by Sc−Te interactions. From this viewpoint one gains the impression that there exist two, to a certain extent uncoupled, electronic systems in this bcc fragment structure, one that provides the electrons for the one-dimensionally extended M−M bonding regions in the metallic core and a second one that may serve as an electron reservoir for additional M−M bonding. This reservoir seems to be nearly empty for Sc_2Te, and almost filled for Zr_2Te.

Structural Comparison. The Sc_2Te type structure seems to allow a considerable amount of flexibility in the number of valence electrons available for homonuclear M−M bonding interactions. This can be seen from the way in which the bonding interactions in Sc_2Te and Zr_2Te adjust to the structure, leaving it topologically intact, instead of forming two different structure

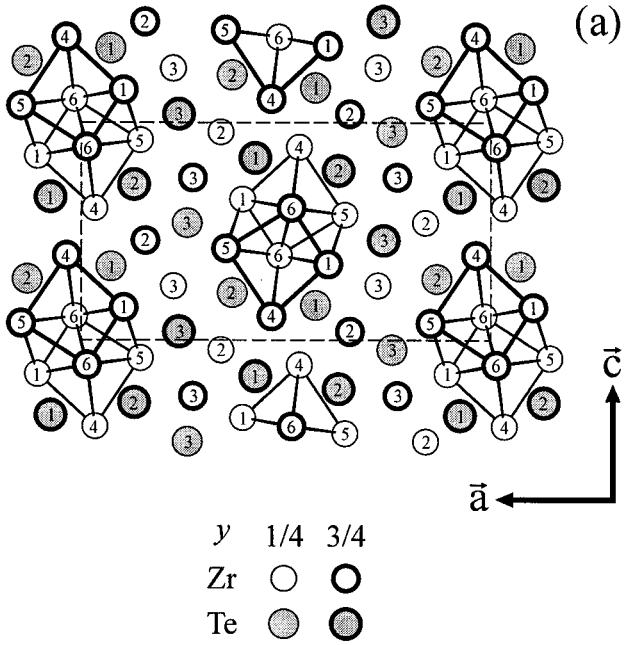

Figure 2. Projection of the Zr_2Te structure along [010]. The unit cell is indicated by a broken line. (a) Pairwise interpenetrating columns of *trans*-face-shared centered Zr_9 cuboids are emphasized. (b) Zr−Zr contacts with a Mulliken overlap population (MOP) > 0.090 are emphasized, revealing the three-dimensional character of the bonding interactions in the metal partial structure of Zr_2Te.

types. Therefore, it is interesting to investigate why the homologous telluride Hf_2Te[14] and the congeneric zirconium selenide Zr_2Se[46] adopt structures which differ from that of Zr_2Te (Figure 6). Obviously there are additional factors conducting the structure type formed in each case.

Let us first examine the distinctions in the structures of Zr_2Te and Hf_2Te, beginning with some remarks concerning the metal-rich chemistry of Zr and Hf. Despite the extensive similarities in the general chemical behavior of the two homologous metals Zr and Hf,[47] stoichiometrically equivalent, metal-rich chalcogenides and pnictides of both metals have, apart from Zr_7P_4[48] and Hf_7P_4,[49] been found to form different structure

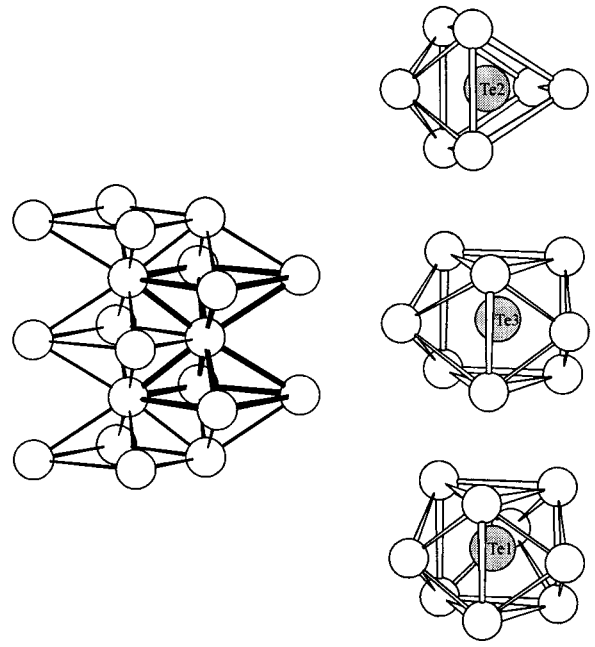

Figure 3. (a) Mutually interpenetrating bcc columns or, alternatively, *cis*-edge-condensed strings of compressed octahedra. A centered Zr_9 cuboid is emphasized. (b) Coordination environments of the Te atoms consist of mono-, bi-, and tricapped distorted trigonal prisms of Zr atoms.

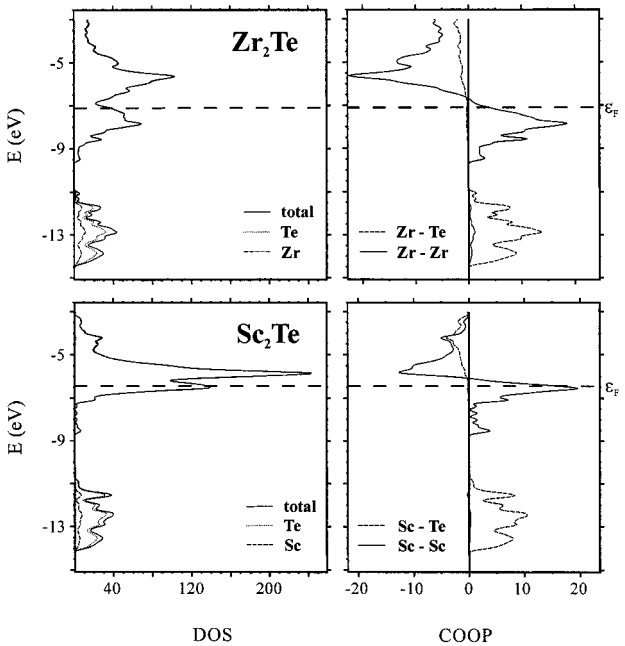

Figure 4. Densities of states (DOS) and crystal orbital overlap population (COOP) curves for Zr_2Te and the isotypic, valence-electron-poorer Sc_2Te. COOP curves for Zr−Te, Zr−Zr, Sc−Te, and Sc−Sc contacts up to 322, 400, 335.2, and 404.9 pm, respectively, are shown. Levels up to the Fermi level (broken, horizontal line) are filled; levels to the right of the vertical line are bonding, to the left are antibonding. The Fermi level for Zr_2Te lies at −7.12 eV, for Sc_2Te at −6.45 eV.

types, e.g., Zr_2Se[46] vs Hf_2Se,[2] and Zr_2P[50] vs Hf_2P.[51] Other metal-rich pnictides and chalcogenides, e.g., Zr_3Te,[13] Hf_3Te_2,[15]

(46) Franzen, H. F.; Norrby, L. J. *Acta Crystallogr.* **1968**, *B24*, 601.
(47) Greenwood, N. N.; Earnshaw, A. *Chemistry of the Elements*, 2nd edition; Butterworth-Heinemann: Oxford, 1997.
(48) Ahlzén, P.-J.; Rundqvist, S. *Z. Kristallogr.* **1989**, *189*, 149.
(49) Kleinke, H.; Franzen, H. F. *Angew. Chem., Int. Ed. Engl.* **1996**, *35*, 1934.
(50) Ahlzén, P.-J.; Rundqvist, S. *Z. Kristallogr.* **1989**, *189*, 117.

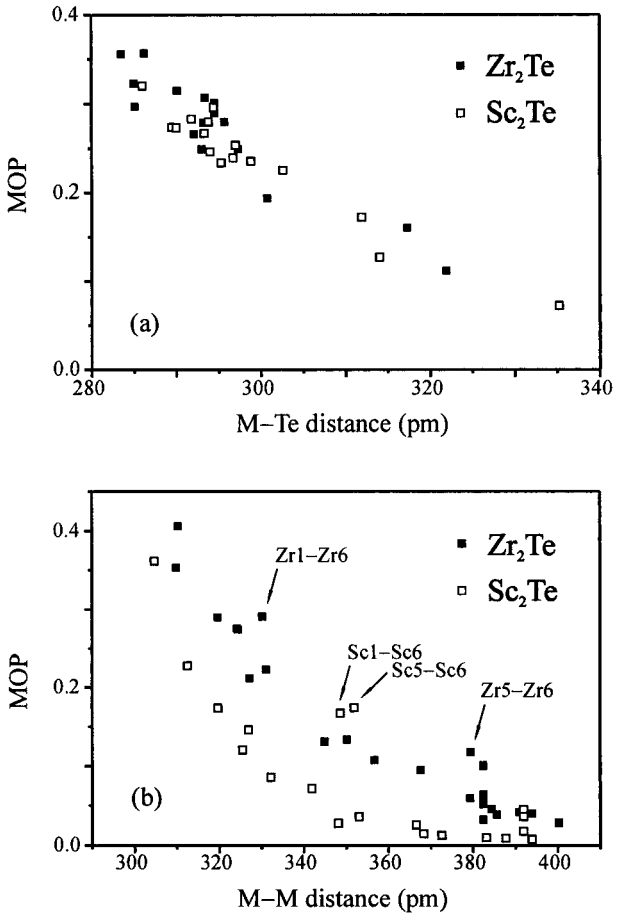

Figure 5. Mulliken Overlap Populations (MOP) in Zr_2Te and Sc_2Te plotted versus (a) M−Te and (b) M−M distance.

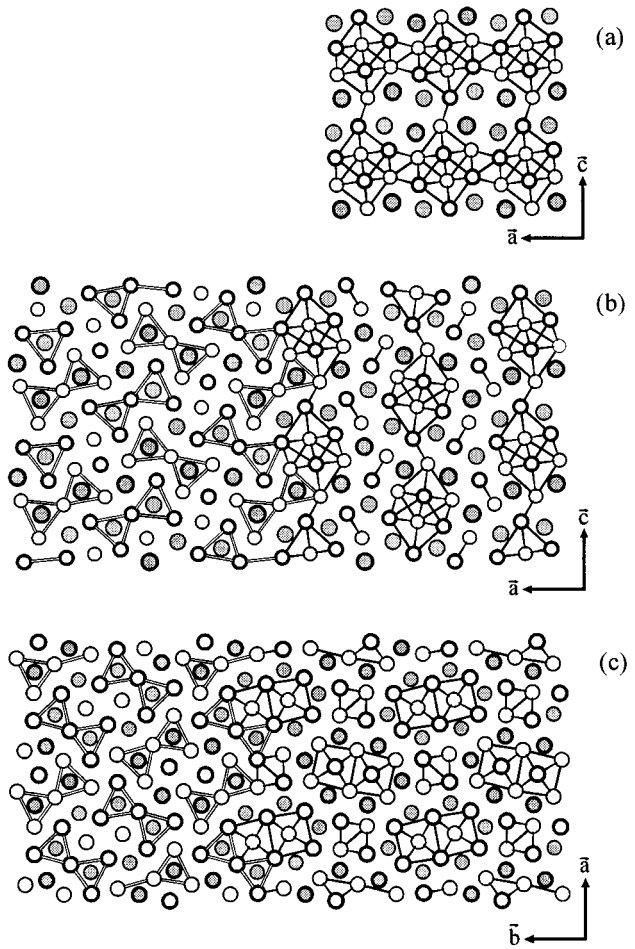

Figure 6. Comparison of the crystal structures of (a) Hf_2Te, (b) Zr_2Te, and (c) Zr_2Se. On the left, twin columns of bi- and tricapped Te centered trigonal Zr prisms are emphasized, whereas on the right the bcc partial structure is stressed. Shaded circles represent chalcogen atoms, open circles represent metal atoms. Thin-bordered circles are located in the plane, thick-bordered at $^1/_2$ lattice parameter above the plane.

$Zr_{14}P_9$,[52] and Hf_3P_2,[53] possess no counterpart of the respective homologous transition metal. In the quasi-binary systems Hf−Zr−P[54] and Ta−Nb−S[55] it has been shown that the 5d metals generally prefer the metal sites which allow more metal−metal bonding. The differences in bonding in metal-rich Zr and Hf phosphides have been extensively discussed before,[49] referring among others to the effects of the greater expansion of the 5d orbitals of Hf compared to the 4d orbitals of Zr, leading to stronger metal−metal bonds and eventually to more metal−metal contacts in Hf compounds. This behavior can be verified with help of the aforementioned M_2X compounds (M = Zr, Hf; X = Se, P) as well as Ta_2Se[16] and Nb_2Se.[5] Accompanying more metal−metal contacts and stronger metal−metal bonds are larger uninterrupted regions consisting solely of metal atoms. As pointed out earlier,[14] this concomitantly leads to a reduction in the average coordination number of the chalcogen or pnicogen atoms involved.

The homologous telluride Hf_2Te[14] (Nb_2Se type)[5] adopts a structure which in its basic assemblage is related to that of Zr_2Te (Figure 6a and b) but nonetheless expressing important differences. The motif of double strings linked in the second dimension over corners appears in both structures. As can be seen in Figure 6 every second one of these "sheets" in Zr_2Te has to be rotated 180° about the *c* axis, shifted by *c*/2 and *b*/2 and connected in the third dimension, leaving out one Te atom (Te3) and the zigzag Zr chain (Zr2 and Zr3), to arrive at the Hf_2Te structure. As opposed to Zr_2Te, Hf_2Te contains no capped trigonal prisms about Te although a related motif can be recognized, the Te coordination representing *hypho*-Hf_6Te fragments of tricapped trigonal prisms, Hf_9Te. Inspecting the metal substructure of Hf_2Te reveals two-dimensional puckered slabs of bcc arrays spreading parallel (001), the Te atoms lining channels extending throughout the structure along [010]. This gives way to a more highly metal−metal bonded structure than in Zr_2Te and is in accordance with the general conclusion that in metal-rich chalcogenides and pnictides of the valence-electron-poor transition metals the 5d metals are more efficient metal−metal bonding elements than the 4d metals.

Comparing Zr_2Te with the congeneric zirconium selenide Zr_2Se[46] (Ta_2P type)[56] is also instructive (Figure 6b and c). Zr atoms on four of the six distinct sites form face-shared double strings of bcc columns, as opposed to the mutually interpenetrating bcc columns found in Zr_2Te. Atoms on the two additional sites form a chain of compressed octahedra sharing edges. The chalcogen atoms are mono-, bi-, and tricapped trigonal prismatically coordinated with Zr. The bi- and tricapped trigonal prisms are also fused over trigonal faces to columns,

(51) Lundström, T.; Ersson, N.-O. *Acta Chem. Scand.* **1968**, *22*, 1801.
(52) Tergenius, L.-R.; Noläng, B.; Lundström, T. *Acta Chem. Scand.* **1981**, *A35*, 693.
(53) Kleinke, H.; Franzen, H. F. *Acta Crystallogr.* **1996**, *C52*, 2127.
(54) Kleinke, H.; Franzen, H. F. *J. Solid State Chem.* **1998**, *136*, 221.
(55) Franzen, H. F.; Köckerling, M. *Prog. Solid St. Chem.* **1995**, *23*, 265.
(56) Nylund, A. *Acta Chem. Scand.* **1966**, *20*, 2393.

the columns being edge condensed to double strings as found in Zr_2Te. The monocapped trigonal prisms lie perpendicular to these strings. This arrangement thus maintains the chalcogen coordination found in Zr_2Te, whereas shorter average Zr−Zr contacts are realized. Compared to Te, the smaller atomic radius of Se probably plays an important role regarding the type of structure formed. Interestingly, Ti_2Se forms both structure types, α-Ti_2Se[57] (Ta_2P type) and β-Ti_2Se[12] (Sc_2Te type), indicating relatively small stability differences between these two structure types. Ti_2Te has not been described in the literature.

Conclusions

The new binary zirconium-rich telluride Zr_2Te has been uncovered and its structure determined by means of X-ray powder diffractometry. Zr_2Te is isostructural with β-Ti_2Se as well as Sc_2Te, which has less valence electrons available for metal−metal bonding. As both Zr and Sc have almost the same atomic radii, the contribution of matrix effects to bonding differences in Zr_2Te and Sc_2Te is minimized and the influence of other factors, such as the number of valence electrons, can be assessed. Therefore, a study of the bonding situation in Zr_2Te and Sc_2Te was undertaken. According to extended Hückel calculations, metal-tellurium bonding interactions are comparable for Sc_2Te and Zr_2Te, whereas metal−metal bonding is anisotropically reduced from a three-dimensional network in Zr_2Te to quasi-one-dimensional units in Sc_2Te. Despite the robustness of the Sc_2Te type structure with respect to variations in the valence electron concentration available for M−M bond formation, the congeneric phases of Zr_2Te, Zr_2Se and Hf_2Te, adopt distinct types of structures.

Acknowledgment. Financial support by the Deutsche Forschungsgemeinschaft is gratefully acknowledged. We thank Holger Kleinke for assistance with the extended Hückel calculations.

Supporting Information Available: A table of relevant parameters of the Rietveld analysis and a table of 2θ-values, indexation, calculated and observed relative X-ray diffraction intensities of Zr_2Te. This material is available free of charge via the Internet at http://pubs.acs.org.

IC990024A

(57) Weirich, T. E.; Pöttgen, R.; Simon, A. *Z. Kristallogr. − NCS* **1996**, *211*, 928.